Inorganic Chemistry

Article

pubs.acs.org/IC

Coordination Polymers Based on Diiron Tetrakis(dithiolato) Bridged by Alkali Metals, Electrical Bistability around Room Temperature, and Strong Antiferromagnetic Coupling

Samia Benmansour,[†] Esther Delgado,*[,‡] Carlos J. Gómez-García,[†] Diego Hernández,[‡] Elisa Hernández,[‡] Avelino Martin,[§] Josefina Perles,[⊥] and Félix Zamora[‡]

[†]Instituto de Ciencia Molecular, Universidad de Valencia, C/Catedrático José Beltrán 2, 46980 Paterna, Valencia, Spain

[‡]Departamento de Química Inorgánica and [⊥]Servicio Interdepartamental de Investigación, Universidad Autónoma de Madrid, 28049 Madrid, Spain

[§]Departamento de Química Inorgánica, Universidad de Alcalá de Henares, Campus Universitario, E-28871 Alcalá de Henares, Spain

Supporting Information

ABSTRACT: Coordination polymer chains have been formed by the direct reaction between $HSC_6H_2Cl_2SH$ and $FeCl_3{\cdot}6H_2O$ in the presence of an aqueous solution of the corresponding alkali-metal hydroxide (M = Li, Na, and K) or carbonate (M = Rb and Cs). The structures consist of dimeric $[Fe_2(SC_6H_2Cl_2S)_4]^{2-}$ entities bridged by $[M_2(THF)_4]$ [M = K (**1**), Rb (**2**), and Cs (**3**); THF = tetrahydrofuran] or $\{[Na_2(\mu\text{-}H_2O)_2(THF)_2]$ (**5** and **5′**) units. The smaller size of the lithium atom yields an anion/cation ion-pair molecule, $[Li(THF)_4]_2[Fe_2(SC_6H_2Cl_2S)_4]$ (**4**), in which the dianionic moieties are held together by Cl···Cl interactions. Electrical characterization of these compounds shows a general semiconductor behavior in which the conductivity and activation energies are mainly determined by the M−Cl and M−S bond distances. Compounds **1** and **5′** are interesting examples of bistability showing reversible transitions centered at ca. 350 and 290 K with very large hysteresis of ca. 60 and 35 K, respectively. All of these compounds exhibit intradimer strong antiferromagnetic Fe···Fe interactions.

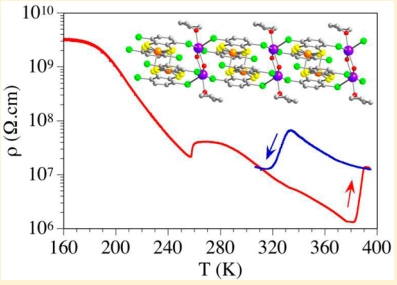

INTRODUCTION

The chemistry of transition-metal complexes with 1,2-dithiolene is still a subject of high research interest going from basic chemical aspects, including the versatility in the coordination modes, their role in crystal engineering, as well as their potential use as mimetic models of the hydrogenase, to their physical properties, such as magnetism and electrical conductivity.[1]

It is known that the presence of donor substituents in the dithiolene ligands may give rise to heterometallic anion−cation chains.[2] Although there are a few examples of transition-metal dithiolene derivatives (M = Ni, Pt, Pd, and Au) where the metal bis(dithiolato) anionic entities are coordinated to alkali metals (Na^+ and K^+) in 1D coordination polymers,[3−6] there is only one example with iron. This compound, formulated as $[K_2(\mu\text{-}H_2O)_2(THF)_4][Fe_2(SC_6H_2Cl_2S)_4]$ (THF = tetrahydrofuran), was recently reported by us[7] and represents the first iron-containing 1D heterometallic coordination polymer. This compound presents a noticeable room temperature conductivity, and its physical properties were rather unexpected: (i) it was the first coordination polymer containing an "s" group metal as a bridging building block showing electrical conductivity; (ii) it represented the first example of a coordination polymer showing two electrical transitions; (iii) both transitions showed large hysteresis and, hence, this compound presents two large domains of bistability. This coordination polymer is isolated from the reaction of $[Fe_2(CO)_6(\mu\text{-}SC_6H_2Cl_2S)]$ with $HSC_6H_2Cl_2SH$, in the presence of K_2CO_3. The interesting results have prompted us to extend the work to evaluate the influence of the use of $FeCl_3{\cdot}6H_2O$ as the starting material instead of the iron carbonyl complex and to evaluate the structural effects of the size of the alkali metals.

Herein we report on the synthesis, characterization, and physical properties of new 1D polymers formed by iron dithiolates connected through alkali-metal ions. These complexes can be formulated as $\{[M_2(THF)_4][Fe_2(SC_6H_2Cl_2S)_4]\}_n$ [M = K (**1**), Rb (**2**), and Cs (**3**)], $[Li(THF)_4]_2[Fe_2(SC_6H_2Cl_2S)_4]$ (**4**), and $\{[Na_2(\mu\text{-}H_2O)_2(THF)_2][Fe_2(SC_6H_2Cl_2S)_4]\}_n$ (**5** and **5′**). Interestingly, compounds **1**−**5′** behave as semiconductors with room temperature electrical conductivity values that strongly depend on the alkali-metal atom and on the M−S and M−Cl bridges connecting the alkali ions with the $[Fe_2(SC_6H_2Cl_2S)_4]^{2-}$ entities. As expected, these compounds exhibit strong intradimer antiferromagnetic Fe···Fe interactions.

Received: November 20, 2014
Published: February 10, 2015

DOI: 10.1021/ic502789v
Inorg. Chem. 2015, 54, 2243−2252

Table 1. Crystal Data and Structure Refinement for Compounds 1−5′

	1	2	3	4	5	5′
moiety	$C_{20}H_{20}Cl_4$	$C_{20}H_{20}Cl_4$	$C_{20}H_{20}Cl_4$	$C_{28}H_{36}Cl_4$	$C_{16}H_{12}Cl_4$	$C_{16}H_{12}Cl_4$
formula	$FeKO_2S_4$	$FeRbO_2S_4$	$FeCsO_2S_4$	$FeLiO_4S_4$	$FeNaO_2S_4$	$FeNaO_2S_4$
fw	657.35	703.72	751.16	769.4	585.14	585.14
T (K)	200	200	200	200	100	150
λ (Å)	0.71073	0.71073	0.71073	0.71073	0.71073	0.71073
cryst syst	triclinic	triclinic	triclinic	triclinic	monoclinic	triclinic
space group	$P\bar{1}$	$P\bar{1}$	$P\bar{1}$	$P\bar{1}$	$C2/c$	$P\bar{1}$
a (Å)	8.358(2)	8.3909(5)	8.340(4)	11.0978(6)	27.083(1)	9.2449(7)
b (Å)	12.207(1)	12.2239(6)	12.086(3)	13.1869(5)	9.1347(5)	12.2060(9)
c (Å)	13.146(3)	13.3861(6)	13.806(6)	13.7014(9)	22.853(1)	19.791(1)
α (deg)	72.89(2)	73.062(4)	74.44(2)	114.408(3)	90	98.708(6)
β (deg)	81.61(2)	81.438(4)	80.27(3)	94.859(5)	103.735(2)	101.342(6)
γ (deg)	86.14(1)	86.627(5)	86.24(3)	107.592(4)	90	97.664(6)
V (Å^3)	1267.7(4)	1298.63(12)	1321.1(9)	1689.03(17)	5492.0(5)	2133.6(3)
Z	2	2	2	2	8	4
μ (mm^{-1})	1.528	3.194	2.667	1.043	1.268	1.632
F(000)	666	702	738	794	2344	1172
cryst size (mm^3)	0.35 × 0.3 × 0.15	0.32 × 0.16 × 0.12	0.28 × 0.24 × 0.16	0.25 × 0.23 × 0.17	0.09 × 0.08 × 0.05	0.20 × 0.19 × 0.17
θ range (deg)	3.06−27.50	3.03−27.5	3.00−27.5	3.00−27.50	1.55−25.38	3.20−25.03
hkl ranges	−10 to +10, −15 to +15, −17 to +17	−10 to +10, −17 to +17, −17 to +17	−10 to +10, −15 to +15, −17 to +17	−14 to +14, −17 to +17, −17 to +17	−32 to +32, −9 to +11, −27 to +27	−10 to +11, −14 to +14, −23 to +23
collected reflns	27678	29730	28612	37190	21990	23124
indep reflns	5800 [R_{int} = 0.073]	5925 [R_{int} = 0.107]	6055 [R_{int} = 0.193]	7746 [R_{int} = 0.173]	5031 [R_{int} = 0.0525]	7515 [R_{int} = 0.0848]
GOF on F^2	1.15	1.07	0.882	1.163	1.000	1.249
final R indices	R1 = 0.066, wR2 = 0.174	R1 = 0.054, wR2 = 0.102	R1 = 0.082, wR2 = 0.195	R1 = 0.080, wR2 = 0.153	R1 = 0.0768, wR2 = 0.2570	R1 = 0.1815, wR2 = 0.4515
R indices [$F > 4\sigma(F)$] (all data)	R1 = 0.096, wR2 = 0.183	R1 = 0.103, wR2 = 0.121	R1 = 0.189, wR2 = 0.251	R1 = 0.201, wR2 = 0.199	R1 = 0.1100, wR2 = 0.2886	R1 = 0.2212, wR2 = 0.4673
largest diff peak/hole (e Å^{-3})	1.275/−0.895	0.809/−0.742	1.349/−3.024	0.758/−0.724	3.508/−1.248	2.063/−1.271

EXPERIMENTAL SECTION

Materials and Methods. All reactions were carried out under an argon atmosphere. All reagents and solvents purchased were used without further purification. Elemental analyses were performed on an LECO CHNS-932 elemental analyzer. Mass spectrometric (MS) measurements recorded in negative and positive electrospray ionization (ESI^- and ESI^+, respectively) mode were obtained on a electrospray QSTAR hybrid quadrupole time-of-flight (Applied Biosystems). Thermogravimetric analysis (TGA) and differential scanning calorimetry (DSC) were recorded in TGA/DSC Q600 TA Instruments.

X-ray Structure Analysis of 1−5′. Single crystals of compounds **1**−**5**′ were covered with a layer of a viscous perfluoropolyether (FomblinY), mounted on a cryoloop (**1**−**4** and **5**′) or a MicroMount (**5**) with the aid of a microscope, and immediately placed in the low-temperature nitrogen stream of the diffractometer. The intensity data sets for complexes **1**−**4** were collected at 200 K on a Bruker-Nonius Kappa CCD diffractometer, while the data sets for compounds **5** and **5**′ were collected at 100 K on a Bruker Kappa Apex II diffractometer (for **5**) and at 150 K on a Supernova diffractometer (for **5**′). All the diffractometers were equipped with Oxford Cryostream units and with graphite-monochromated (enhanced for **5**′) Mo Kα radiation (λ = 0.71073 Å). The structures were solved using the *WINGX*[8] package for **1**−**4**, *SHELXTL*[9] for **5**, and *CRYSALIS*[10] for **5**′ by Patterson (**1**−**4**) or direct methods (**5** and **5**′) (*SHELXS-97* for **1**, **3**, **5**, and **5**′ and *SHELXS-2013* for **2** and **4**) and refined by least squares against F^2 (*SHELXL-97* for **1**, **3**, **5**, and **5**′ and *SHELXL-2013* for **2** and **4**).[11] Empirical absorption correction was performed using spherical harmonics, implemented in the *SCALE3 ABSPACK* scaling algorithm. All non-hydrogen atoms were anisotropically refined. The hydrogen atoms were positioned geometrically and refined using a riding model. The crystal data are shown in Table 1.

Direct-Current (dc) Conductivity Measurements. The thermal dependence of dc electrical conductivity was measured with the four (or two, depending on the size of the crystals) contacts method on several (at least four) single crystals of compounds **1**−**5**′ in the temperature range 2−400 K. All the samples were measured at least once with each method, and after verifying that the results were similar, within experimental error, we decided to use the two-contacts method for simplicity. The contacts were made with platinum wires (25 μm diameter) using graphite paste. The samples were measured in a Quantum Design PPMS-9 instrument connected to an external voltage source (Keithley model 2400 sourcemeter) and amperometer (Keithley model 6514 electrometer). All the conductivity quoted values were measured in the voltage range where the crystals are ohmic conductors. The cooling and warming rates were 0.5 and 1 K min^{-1}.

Magnetic Measurements. Magnetic susceptibility measurements were carried out in the temperature range 2−300 K with an applied magnetic field of 0.5 T on polycrystalline samples of **1**−**5** (with masses of 23.52, 6.92, 19.55, 39.68, and 12.43 mg, respectively) with a Quantum Design MPMS-XL-5 SQUID susceptometer. The susceptibility data were corrected for the sample holders previously measured using the same conditions and for the diamagnetic contributions of the salt as deduced using Pascal's constant tables (χ_{dia} = −636 × 10^{-6}, −558 × 10^{-6}, −583.5 × 10^{-6}, −541 × 10^{-6}, and −606 × 10^{-6} cm^3 mol^{-1} for **1**−**5**). The magnetic properties of compound **5**′ could not be carried out because we could only obtain a few crystals of this polymorph.

Syntheses of Compounds $\{[M_2(THF)_4][Fe_2(SC_6H_2Cl_2S)_4]\}_n$ [(M = K (1), Rb (2), and Cs (3)]. 1,2-$HSC_6H_2Cl_2SH$ (156 mg, 0.74 mmol) was treated with an aqueous solution (10 mL) of KOH, Rb_2CO_3, or Cs_2CO_3 (5% by weight). Then, $FeCl_3{\cdot}6H_2O$ (100 mg, 0.37 mmol) in 10 mL of ethanol/water (1:1) was slowly added. The mixture was stirred at room temperature for 30 min. The solid formed was collected by filtration and washed several times with water and dichloromethane. Suitable crystals for X-ray analysis of compounds

DOI: 10.1021/ic502789v
Inorg. Chem. 2015, 54, 2243−2252

$\{[K_2(THF)_4][Fe_2(SC_6H_2Cl_2S)_4]\}_n$ (**1**; 185 mg, 48% yield) and $\{[Rb_2(THF)_4][Fe_2(SC_6H_2Cl_2S)_4]\}_n$ (**2**; 235 mg, 38.2% yield) were obtained from a solution of THF/*n*-hexane (1:1) of 24 and 30 mL for **1** and **2**, respectively, at room temperature, while compound $\{[Cs_2(THF)_4][Fe_2(SC_6H_2Cl_2S)_4]\}_n$ (**3**) was isolated from a solution of THF/*n*-heptane (1:1) of 50 mL at the same temperature (70 mg, 31% yield). Compound **1**. ESI^--MS (MeOH, *m*/*z*): 473.7 ($[Fe(SC_6H_2Cl_2S)_2]^-$), 947.5 ($[Fe_2(SC_6H_2Cl_2S)_4]^-$), 986.4 ($[KFe_2(SC_6H_2Cl_2S)_4]^-$). Anal. Calcd for $C_{36}H_{32}Cl_8Fe_2K_2S_8O_3$: C, 34.79; H, 2.57; S, 20.60. Found: C, 33.73; H, 2.96; S, 20.78. Compound **2**. ESI^--MS (MeCN, *m*/*z*): 473.7 ($[Fe(SC_6H_2Cl_2S)_2]^-$), 947.5 ($[Fe_2(SC_6H_2Cl_2S)_4]^-$). ESI^+-MS (MeCN, *m*/*z*): 84.9 ($[Rb]^+$). Anal. Calcd for $C_{40}H_{40}Cl_8Fe_2Rb_2S_8O_4$: C, 34.13; H, 2.86; S, 18.23. Found: C, 34.02; H, 3.00; S, 18.87. Compound **3**. ESI^--MS (MeOH, *m*/*z*): 473.7 ($[Fe(SC_6H_2Cl_2S)_2]^-$). ESI^+-MS (MeCN, *m*/*z*): 132.9 ($[Cs]^+$). Anal. Calcd for $C_{36}H_{32}Cl_8Fe_2Cs_2S_8O_3$: C, 30.23; H, 2.24; S, 17.90. Found: C, 29.44; H, 2.23; S, 17.87.

Synthesis of $[Li(THF)_4]_2[Fe_2(SC_6H_2Cl_2S)_4]$ (4). The reaction was carried out following the same procedure but using LiOH as the starting material. Suitable crystals for X-ray analysis of compound **4** were obtained from a solution of THF/*n*-hexane (1:1) of 20 mL at room temperature. (170 mg, 40.2% yield). ESI^+-MS (MeOH, *m*/*z*): 473.7 ($[Fe(SC_6H_2Cl_2S)_2]^-$), 947.5 ($[Fe_2(SC_6H_2Cl_2S)_4]^-$). ESI^--MS (MeOH, *m*/*z*): 968.5 ($[Li_3Fe_2(SC_6H_2Cl_2S)_4]^+$), 1000.5 ($[Li_3Fe_2(SC_6H_2Cl_2S)_4\cdot MeOH]^+$). Anal. Calcd for $C_{56}H_{72}Cl_8Fe_2Li_2S_8O_8$: C, 43.71; H, 4.72; S, 16.67. Found: C, 43.25; H, 4.77; S, 16.62.

Synthesis of $\{[Na_2(\mu\text{-}H_2O)_2(THF)_2][Fe_2(SC_6H_2Cl_2S)_4]\}_n$ (5). The reaction was carried out following the same procedure but using NaOH as the starting material. The residue was recrystallized from THF/*n*-heptane (1:1) of 20 mL at room temperature, yielding suitable crystals for single X-ray diffraction studies (190 mg, 34.8% yield). ESI^--MS (MeOH, *m*/*z*): 473.7 ($[Fe(SC_6H_2Cl_2S)_2]^-$), 947.5 ($[Fe_2(SC_6H_2Cl_2S)_4]^-$). Anal. Calcd for $C_{32}H_{28}Cl_8Fe_2Na_2S_8O_4$: C, 32.73; H, 2.40; S, 21.84. Found: C, 32.56; H, 2.86; S, 21.48.

RESULTS AND DISCUSSION

Synthesis and Structural Characterization. Recently, we have obtained the first 1D polymer built by anionic iron dithiolato entities and potassium cations $\{[K_2(\mu\text{-}H_2O)_2(THF)_4][Fe_2(SC_6H_2Cl_2S)_4]\}_n$ (**6**),[7] using the organometallic compound $[Fe_2(CO)_6(\mu\text{-}SC_6H_2Cl_2S)]$ as the starting material. Here we extend this study to all alkali-metal ions, and we prove that $FeCl_3\cdot 6H_2O$ can also be used as an iron source for the preparation of coordination polymers in the presence of different alkali metals. Thus, direct reactions between 1,2-$HSC_6H_2Cl_2SH$ and $FeCl_3\cdot 6H_2O$ in the presence of the corresponding alkali bases lead to the formation of a series of 1D coordination polymers and a molecular $[Li(THF)_4]_2[Fe_2(SC_6H_2Cl_2S)_4]$ complex.

The crystal structure of compound **1** (Figure 1) consists of anionic $[Fe_2(SC_6H_2Cl_2S)_4]^{2-}$ moieties connected through potassium atoms. The K^+ ions form dimers linked through a double sulfur bridge from two different $[Fe_2(SC_6H_2Cl_2S)_4]^{2-}$ moieties. Figure 1 shows the basic unit of the polymer in which each K^+ ion is coordinated by two sulfur atoms (S2 and S3) and two chlorine atoms (Cl2 and Cl4) from one dimeric $[Fe_2(SC_6H_2Cl_2S)_4]^{2-}$ moiety, two oxygen atoms from two THF molecules (O1 and O2), and a sulfur atom (S2) from a second anionic $[Fe_2(SC_6H_2Cl_2S)_4]^{2-}$ moiety, resulting in a distorted monocapped octahedral geometry.

The anions display the same geometry as that previously found in the related compound **6**,[7] where each iron atom shows the expected 4 + 1 square-pyramidal geometry. This is the typical coordination mode shown by most of the iron bis(dithiolato) compounds. Each of these dimetallic anions is

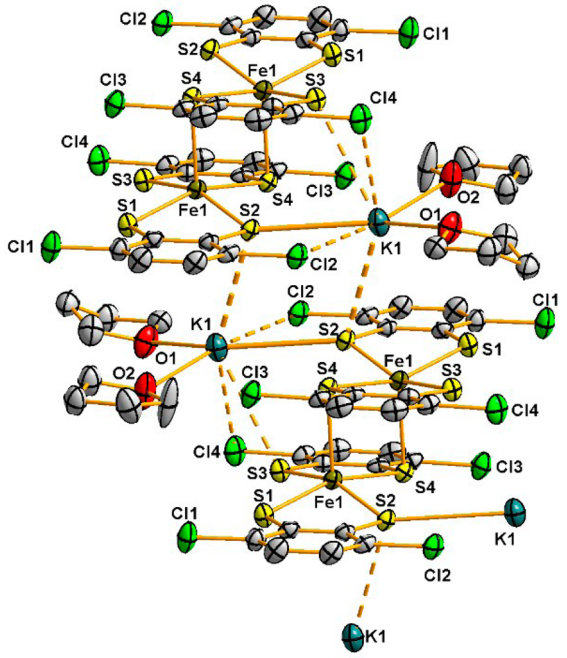

Figure 1. ORTEP drawing showing the labeling scheme of compound **1**.

connected to two adjacent K^+ cations by S−K and Cl−K bonds (Table 2), forming chains in the [100] direction (Figure 2). Note that this structure is similar to that found[7] in compound **6**, although in **1**, the K^+ ions are bridged by two sulfur atoms instead of two water molecules.

Compounds **2** and **3** show the formation of 1D coordination polymers similar to that previously described for **1** (Figure 2). In both compounds, the cations also form dimers connected through a double sulfur bridge from two different $[Fe_2(SC_6H_2Cl_2S)_4]^{2-}$ moieties. While the Rb^+ ion exhibits the same coordination environment as that found for the K^+ ion (Figure 3a), given the larger size of Cs^+ compared with those of K^+ and Rb^+, the cations in compound **3** show a coordination number of 8 instead of 7 with a bicapped trigonal-antiprismatic geometry (Figure 3b). Thus, in **3**, each Cs^+ is surrounded by a total of four sulfur atoms (S1, S3, S4, and S4*) compared to three (S2, S2*, and S3) in **1** and **2**.

To complete this study, we have evaluated the role of the smaller alkali metals such as lithium and sodium. The crystal structure of compound **4** (Figure 4) shows two important differences with the previously described structures of compounds **1**−**3**: (i) The Li^+ cations in **4** do not form any dimer but discrete $[Li(THF)_4]^+$ monomers. (ii) The $[Fe_2(SC_6H_2Cl_2S)_4]^{2-}$ moieties, which are similar to those found in compounds **1**−**3**, are not connected by M^+ dimers but through a direct Cl···Cl interaction of 3.594 Å, giving rise to regular chains along the *a* axis. These two differences have to be attributed to the much smaller size of Li^+ compared to those of K^+, Rb^+, and Cs^+.

The crystal structure of compound **5** (Figure 5) is very similar to those of compounds **1**−**3**, although there is one important difference: the dimers formed by the Na^+ cations are not connected through a double sulfur bridge but by two water molecules. This difference is probably due to the intermediate size of the Na^+ cations, too small to form the double sulfur bridge but big enough to form a double water bridge. Interestingly, K^+ (slightly bigger that Na^+) may also form a

DOI: 10.1021/ic502789v
Inorg. Chem. 2015, 54, 2243−2252

Table 2. Selected Bond Distances (Å) for Compounds 1−5′

	1	2	3	4	5	5′[a]
M−O	2.687(5)	2.822(4)	2.95(1)	1.88(1)	2.237(8)	2.33(2)/2.26(2)
	2.645(5)	2.802(4)	3.016(9)	1.91(1)1.94(1)	2.352(7)	2.34(2)/2.41(2)
				1.94(1)	2.442(6)	2.37(3)/2.48(2)
M−S	3.251(2)	3.350(1)	3.495(3)		2.964(4)	2.98(1)/2.98(1)
	3.418(2)	3.496(1)	3.601(3)		3.191(4)	3.21(1)/3.22(1)
	3.515(2)	3.604(1)	3.649(3)			
			3.810(3)			
M−Cl	3.339(2)	3.491(1)	3.736(3)		3.177(4)	3.10(1)/3.09(1)
	3.501(2)	3.603(2)	3.741(3)		3.203(4)	3.21(1)/3.19(1)
Fe−S	2.214(2)	2.219(1)	2.184(3)	2.220(2)	2.204(2)	2.200(7)/2.203(6)
	2.222(2)	2.224(1)	2.191(3)	2.222(2)	2.214(2)	2.205(8)/2.217(6)
	2.223(2)	2.231(1)	2.257(3)	2.223(2)	2.220(2)	2.215(7)/2.229(6)
	2.227(2)	2.231(1)	2.265(3)	2.230(2)	2.228(2)	2.230(7)/2.235(6)
	2.454(2)	2.461(1)	2.459(3)	2.482(2)	2.486(2)	2.503(7)/2.483/7)

[a]In this compound, there are two crystallographically independent sodium and iron atoms.

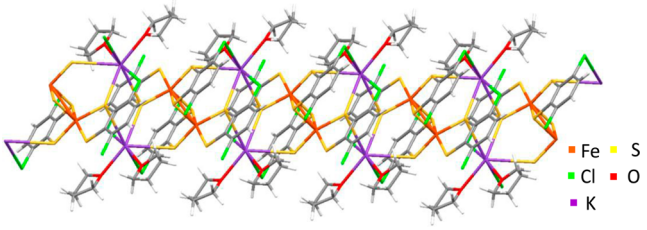

Figure 2. View of a polymer chain of **1** along the *a* axis.

double aquo-bridged dimer, as observed in compound **6**,[7] as well as a double sulfur-bridged dimer, as observed in **1**. Each Na^+ cation is surrounded by seven donor atoms: three oxygen atoms (O1 and O1*, from the two bridging water molecules and O2 from a THF molecule), two sulfur atoms (S3 and S4) from two different $[Fe_2(SC_6H_2Cl_2S)_4]^{2-}$ moieties, and two chlorine atoms (Cl3 and Cl4) from two different anions, resulting in a highly distorted pentagonal-bipyramidal geometry.

In the crystallization process of compound **5**, a few crystals of the polymorph **5′** were obtained. They show different crystal

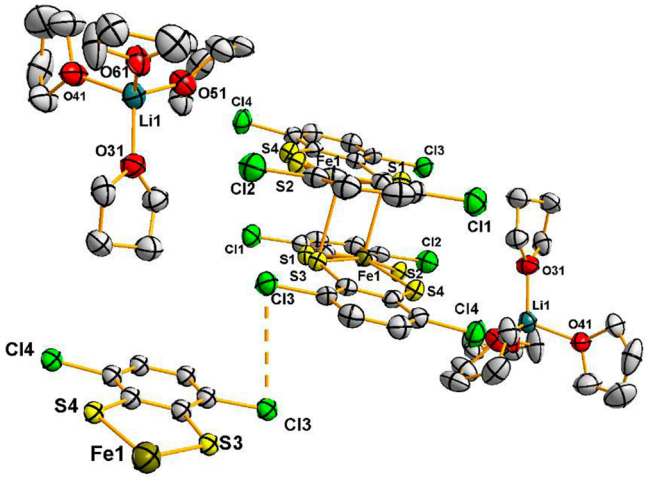

Figure 4. ORTEP drawing showing the labeling scheme of compound **4**.

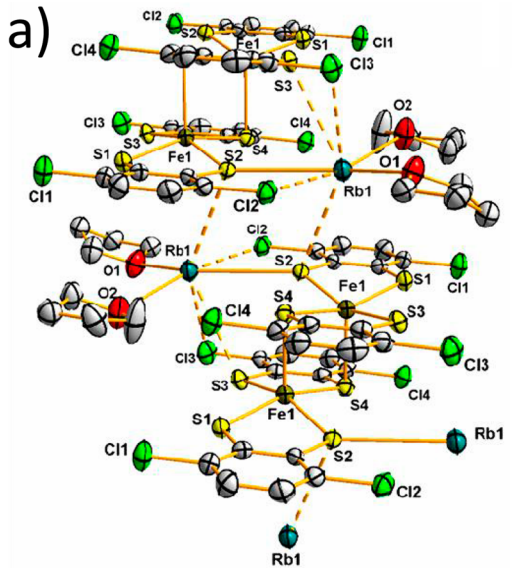

Figure 3. ORTEP drawing showing the labeling scheme of compounds **2** (a) and **3** (b).

DOI: 10.1021/ic502789v
Inorg. Chem. 2015, 54, 2243−2252

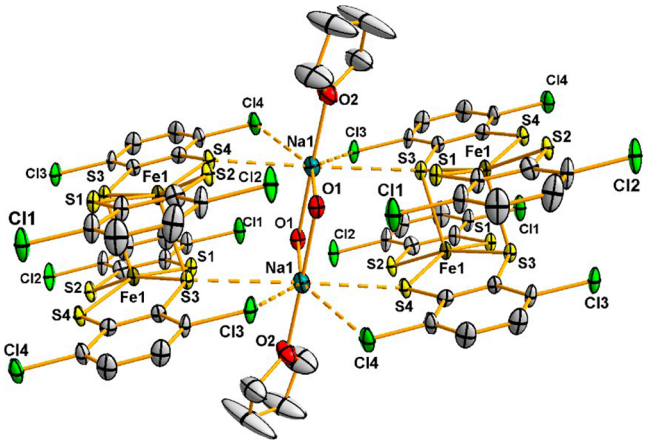

Figure 5. ORTEP drawing showing the labeling scheme of compound **5**.

packing as a consequence of the orientation of the THF ligands coordinated to the Na^+ cations. Thus, in **5** they are located parallel to the molecular axis connecting one bridging water molecule (O1), the Na^+ ion, and the oxygen atom of the THF ligand (O2) (Figure 6a), while in **5′** the THF molecules are

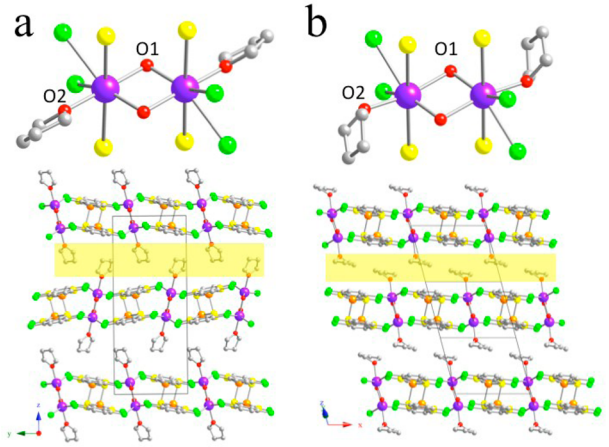

Figure 6. View of the $[Na_2(\mu\text{-}H_2O)_2(THF)_2]^{2+}$ dimers with the relative orientation of the THF ligands (up) and of the interchains interactions of these THF ligands (in yellow, down) in **5** (a) and **5′** (b). Hydrogen atoms are omitted for clarity. Color code: iron, orange; sodium, purple; carbon, green; sulfur, yellow; chlorine, gray; oxygen, red.

almost perpendicular to the same axis (Figure 6b). As a consequence, important differences in the interchain interactions in both compounds are observed (Figure 6).

The structures of compounds **5** and **5′** show some remarkable features: (i) they are a couple of polymorphs with a very different crystal symmetry (**5** is monoclinic, whereas **5′** is triclinic) but presenting the same chain structure; (ii) they contain a double aquo bridge connecting the two alkali metal atoms, in contrast to the other compounds reported here, that present a double sulfur bridge; (iii) they constitute, therefore, a unique example to study the influence on the electrical properties (see below) of small changes in the bond distances along the chain while keeping the composition and structure constant. Furthermore, compounds **5** and **5′** are, together with the related compound **6**,[7] the only ones containing a double aquo bridge connecting the alkali metal. Note that the only metals giving rise to these aquo bridges, Na^+ (in **5** and **5′**) and K^+ (in **6**), are those with intermediate sizes and with a higher trend to coordinate water molecules among the alkali metals.

All of these observations lead to the conclusion that the size of the alkali-metal ion determines the type of structure obtained: (i) isolated $[M(THF)_4]^+$ complexes (for the small Li^+ ion in **4**), (ii) double aquo-bridged $[M_2(\mu\text{-}H_2O)_2(THF)_2]^{2+}$ dimers (M = Na^+ in **5** and **5′** and K^+ in **6**),[7] and (iii) double sulfur-bridged $[M_2(\mu\text{-}S)_2(THF)_4]^{2+}$ dimers (M = K^+ in **1**, Rb^+ in **2**, and Cs^+ in **3**). This key role of the alkali-metal ion is also observed in their coordination numbers (4, 7, 7, 7, and 8 for lithium, sodium, potassium, rubidium, and cesium, respectively).

A search in the CCDC database (updated Nov 2014) shows a total of 21 structures with C−Cl···K bonds, all in the range 3.143−3.674 Å with an average value of 3.40 Å.[7,12] There is only one example of C−Cl···Rb bond, with a Cl···Rb distance of 3.449 Å.[13] There are seven structures with C−Cl···Cs bonds all in the range 3.456−3.821 Å and with an average value of 3.64 Å.[14] Finally, there are seven structures with C−Cl···Na bonds, all in the range 2.983−3.298 Å and with an average value of 3.09 Å.[15] All of the observed Cl···M bonds in compounds **1**−**3**, **5**, and **5′** (Table 2) lie in the corresponding ranges and are close to the average values, confirming the existence of these Cl···M bonds. Note also that most of the reported examples in the CCDC database correspond to Cl atoms directly connected to aromatic rings (as in compounds **1**−**3**, **5**, and **5′**).

Finally, it is worth noting that, although there are ca. 20000 reported complexes containing alkali-metal ions, surprisingly, the coordination environments found in compounds **1**−**3** and **5** are extremely unusual. In fact, a search in the CCDC database shows only one example of heptacoordinated K^+ ions surrounded by three sulfur, two chlorine, and two oxygen atoms $\{KS_3Cl_2O_2\}$,[12i] as observed in **1**. To our surprise, the CCDC database shows no examples of $\{RbS_3Cl_2O_2\}$, $\{CsS_4Cl_2O_2\}$, or $\{NaS_2O_3Cl_2\}$ coordination spheres as observed in **2**, **3**, and **5** (or **5′**), respectively, confirming the uniqueness of these compounds. Only compound **4** presents a well-known $\{LiO_4\}$ coordination environment for the alkali cation.

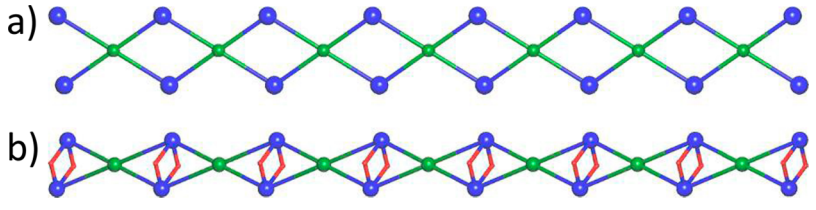

Figure 7. Underlying nets found in compounds **1**−**3** (a) and **5** and **5′** (b). $[Fe_2(S_2C_6H_2Cl_2)_4]^{2-}$ anions are depicted as green spheres, M^+ cations are in blue, and water ligands are in red.

DOI: 10.1021/ic502789v
Inorg. Chem. 2015, 54, 2243−2252

Table 3. Room Temperature dc Conductivity Values, Activation Energies, and Transition Temperatures for Compounds 1−5′

compound	scan[a]	$\sigma_{300\ K}$ (S/cm)	E_a (meV)	T_c[b](K)	T_c[c](K)
1	1c	8×10^{-6}	216	290	
	2w	7×10^{-6}	232	252	384
	3c	9×10^{-8}	297	280	353
	4w	5×10^{-8}	310	253	389
	5c	7×10^{-8}			327
2	1c	4×10^{-8}	210		
	2w	4×10^{-8}	260	263	- 361
	3c		1218		
3	1c	5×10^{-8}	1030	255−280	322
	2w	1×10^{-6}	1070	250−260	
	3c	1×10^{-7}	1070/1080	257−298	334
	4w	4×10^{-7}	1860	256−264	
	5c	3×10^{-8}	1090		
4	1c	5×10^{-9}	319		
	2w	4×10^{-9}	877/457/243	246−263	310−355
	3c	6×10^{-8}	332	242	294−363
	4w	4×10^{-8}	570/787/534	245	277
5	1c	1×10^{-8}	290		
	2w	1×10^{-8}	825/1088/438	270	350
	3c	9×10^{-9}	421/294		315
	4w	5×10^{-9}	585/427/426	280	356
	5c	9×10^{-10}	410		318
	6w	6×10^{-10}	773/556/442	280	332
	7c	6×10^{-10}	417		320
5′	1c	1×10^{-7}	398		
	2w	3×10^{-6}	452/464	275	
	3c	2×10^{-7}	310/634	305	
	4w	2×10^{-6}	252/385/702	276	
	5c	2×10^{-7}	306/286/453	305	
	6w	1×10^{-6}	219/387/576	282	
	7c	4×10^{-7}	265/394	304	
	8w	1×10^{-6}	261/355/478	283	
	9c	2×10^{-7}	349/308/423	303	

[a]c = cooling; w = warming. [b]Low-temperature transition. [c]High-temperature transition.

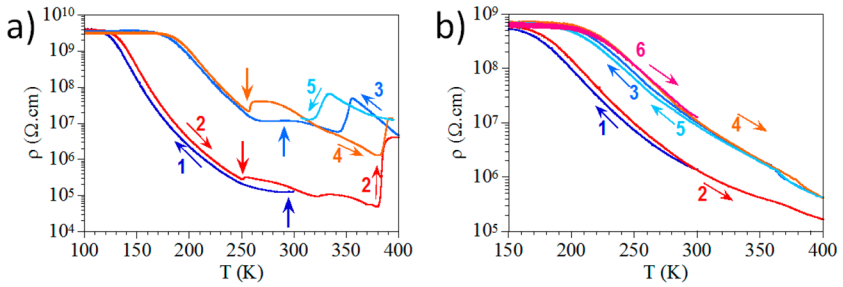

Figure 8. Thermal variation of the resistivity (logarithmic scale) of compounds **1** (a) and **2** (b) during several cooling and warming cycles in the temperature range 100−400 K. Vertical arrows indicate the low-temperature transitions. The numbers indicate the order of the thermal scans. The horizontal saturation at low temperatures indicates that the resistance has reached the measuring limit of our equipment (ca. 5×10^{11} Ω).

Table 2 displays some selected bond distances and angles corresponding to compounds **1**−**5**′. These data show that the basal Fe−S bond distances range from 2.184(3) to 2.265(3) Å and are shorter than the axial ones, 2.454(2) to 2.503(7) Å, as observed in many other dimeric iron bis(dithiolato) complexes, including the related compound **6**:[7] $[n\text{-NBu}_4]_2[\text{Fe(cbdt)}_2]_2$ (cbdt = 4-cyanobenzene-1,2-dithiolato),[16] $[n\text{-NBu}_4]_2[\text{Fe(dcbdt)}_2]_2$ (dcbdt = 4,5-dicyanobenzene-1,2-dithiolato),[17] $[\text{AsPh}_4]_2[\text{Fe(qdt)}_2]_2$ (qdt = quinoxalinedithiolato),[16] and $[\text{NHEt}_3]_2[\text{Fe(pdt)}_2]_2$ (pdt = pyrazine-2,3-dithiolato).[18] The M−Cl, M−S, and M−O bond distances (M = alkali cations) in compounds **1**−**5**′ (Table 2) are in the range found in other related species.[19]

A comparative topological study for the polymeric compounds **1**−**3**, **5**, and **5**′ considering both the dimetallic anionic units and the M^+ cations as nodes shows that the underlying net found in structures **1**−**3** is a monodimensional 2,4-connected $(4^2)(4)_2$ binodal net (Figure 7a). However, the underlying net in the structures of **5** and **5**′ incorporates the bridging water molecules as 2-connected nodes and is a 2,4,4-connected 3-nodal monodimensional net with symbol (4^2)-$(4^6)_2(4)_2$ (Figure 7b).

DOI: 10.1021/ic502789v
Inorg. Chem. 2015, 54, 2243−2252

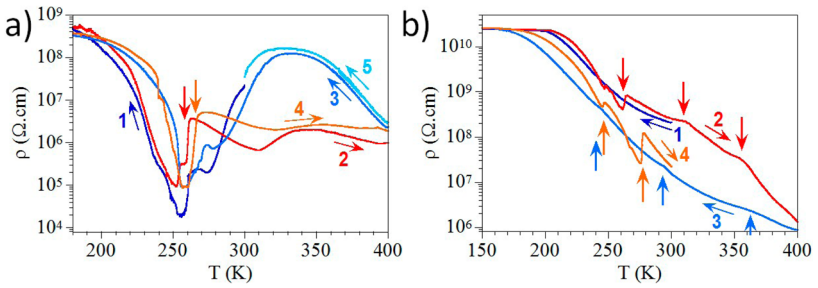

Figure 9. Thermal variation of the resistivity (logarithmic scale) of compounds **3** (a) and **4** (b). Vertical arrows indicate the transitions. The numbers indicate the order of the thermal scans. The horizontal saturation at low temperatures indicates that the resistance has reached the measuring limit of our equipment (ca. 5×10^{11} Ω).

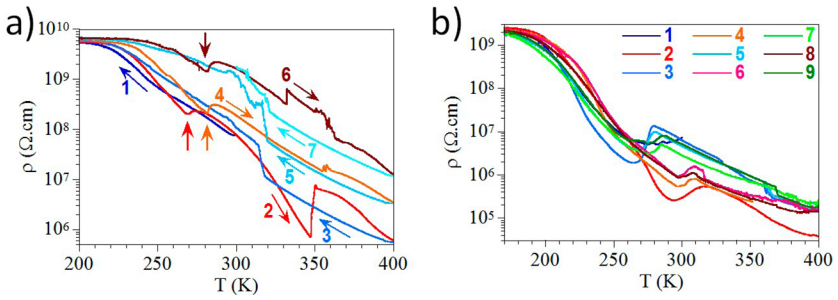

Figure 10. Thermal variation of the resistivity (logarithmic scale) of compounds **5** (a) and **5′** (b). Vertical arrows indicate the low-temperature transitions. The numbers indicate the order of the cooling (1, 3, 5, 7, and 9) and warming (2, 4, 6, and 8) scans. The horizontal saturation at low temperatures indicates that the resistance has reached the measuring limit of our equipment (ca. 5×10^{11} Ω).

Electrical Properties. The dc electrical properties of complexes **1**−**5′** show that they are all semiconductors although, as expected, the conductivity values and activation energies strongly depend on the alkali-metal ion and on the structural features (Table 3).

Compound **1** shows at room temperature a conductivity value of ca. 8×10^{-6} S/cm (Table 3 and Figure 8a) that decreases when **1** is cooled, showing a semiconducting behavior with an activation energy of 216 meV (Figure S1 in the SI) and reaching the detection limit of our equipment (5×10^{11} Ω) at ca. 120 K. When the sample is heated, the resistivity shows a sharp increase at ca. 384 K, suggesting the presence of a transition to a low-conductivity phase. After this initial heating, when the crystal is cooled; this abrupt transition is observed at ca. 353 K (i.e., with a hysteresis of ca. 31 K); although the resistivity does not recover the initial values observed before the transition. This fact suggests that this transition also implies a partial degradation of the crystal, in agreement with the increase observed in the activation energy after each thermal cycle (from 216 to 232, 297, and 310 meV; Figure S1 in the SI). During the second warming/cooling scan, this reversible transition is again observed, although at higher and lower temperatures (ca. 389 and 327 K) with a much higher hysteresis of ca. 62 K. A close look at the 250−300 K region shows that there is a second tiny transition taking place at ca. 250 K in the warming scans and ca. 280−290 K in the cooling ones. This second transition is very smooth, but it is clearly observed in both cycles (vertical arrows in Figure 8a). This behavior is identical with the one observed in the related compound **6** that presents a very similar chain structure.[7] As in the case of compound **6**, we can attribute this original behavior to the coexistence of two different semiconducting states with a very low energy difference.

Compound **2** shows a room temperature conductivity value of ca. 7×10^{-7} S/cm (Table 3 and Figure 8b) that also decreases as the temperature decreases, in a classical semiconducting behavior, with an activation energy of 227 meV (Figure S2 in the SI) and reaches the limit of our equipment at ca. 150 K. In the successive warming and cooling scans, compound **2** shows a slight degradation and a similar semiconducting behavior but no transition at low or high temperatures (Figure 8b).

Compound **3** shows at room temperature a conductivity value of ca. 5×10^{-8} S/cm (Table 3 and Figure 9a) that increases as the temperature decreases with a maximum slope at ca. 280 K. At ca. 255 K, the resistivity reaches a deep minimum with a value of ca. 5×10^{-5} S/cm. Below ca. 255 K, the resistivity increases again in a classical semiconducting way with a high activation energy of ca. 1030 meV (Figure S3 in the SI). Below ca. 180 K, the resistivity reaches the limit of our equipment. The consecutive warming and cooling scans show again the presence of a deep minimum in the resistivity at ca. 250−270 K and a second softer increase at ca. 330 K in the warming scans and a broad maximum at ca. 330 K in the cooling ones. In contrast to compounds **1** and **2**, there is no degradation of the crystals during the warming scans in compound **3**. These data resemble those observed in compounds **1** and **6**, although in **3**, the transition at ca. 250 K is much deeper. Again, as in compounds **1** and **6**, these transitions indicate the existence of two different states with very low energy differences.

Compound **4** shows at room temperature a conductivity of 5×10^{-9} S/cm (Figure 9b and Table 3). When compound **4** is cooled, the resistivity increases in a classical semiconducting way with an activation energy of 319 meV (Figure S4 in the SI) and reaches the limit of our equipment at ca. 200 K. In the successive warming scans, compound **4** shows a classical

DOI: 10.1021/ic502789v
Inorg. Chem. 2015, 54, 2243−2252

semiconducting behavior with activation energies in the range 243−877 meV (Figure S4 in the SI and Table 3) and with tiny transitions observed as minima at ca. 250−260 K or small changes in the slope at ca. 310 and 355 K (Figure 9b). These transitions resemble those observed in compounds **1**, **3**, and **6**, although in **4**, the transitions are very tiny. As in compound **3**, the sample shows no degradation after being heated at 400 K. Even more, in the cooling scan, it shows an even higher conductivity value at room temperature of ca. 6×10^{-8} S/cm. This behavior is slightly different from that found in compounds **1**−**3** and **6** because now the sample improves its conductivity after heating at 400 K, and the transitions are smoother than those observed in **1**−**3** and **6**. This result, together with the lower conductivity value of **4**, can be attributed to the different structure observed in **4** (see above). Thus, **4** is the only compound where the alkali metal is not connecting the $[Fe_2(SC_6H_2Cl_2S)_4]^{2-}$ dimers to generate chains. In fact, the conductivity in **4** has to be attributed to the formation of chains of $[Fe_2(SC_6H_2Cl_2S)_4]^{2-}$ dimers connected through moderate Cl···Cl interactions along the *a* axis. The slight increase of the conductivity observed after heating the crystals may be due to an annealing process that results in a shortening of the Cl···Cl distances (i.e., upon heating, the crystals relax to a slightly more compact and stable structure).

Compound **5** shows at room temperature a conductivity value of 1×10^{-8} S/cm that decreases when it is cooled, showing a classical semiconducting behavior (Figure 10a and Table 3) with an activation energy of 290 meV (Figure S5 in the SI). Below ca. 200 K, the resistivity reaches the limit of our equipment. Compound **5** shows a behavior very similar to that of compound **4**, with tiny transitions observed as minima in the warming scans at ca. 270 and 350 K and as sharp increases in the resistivity at ca. 320 K in the cooling scans. After the sample is heated at 400 K, it shows a progressive degradation and, accordingly, the resistivity becomes higher after each scan, as observed in compounds **1**, **2**, and **6**.

The polymorph **5′** presents a behavior similar to that of compound **5**, although with a higher room temperature conductivity of ca. 1×10^{-6} S/cm (Figure 10b and Table 3). When the sample is cooled, the resistivity shows a semiconducting behavior with an activation energy of 398 meV (Figure S6 in the SI) and shows a progressive smooth transition at ca. 290 K. Below ca. 180 K, the resistivity reaches the limit of our equipment. In the successive warming and cooling scans, compound **5′** shows a smooth reversible transition at ca. 310 K in the warming scans and at ca. 275 K in the cooling ones with a hysteresis of ca. 35 K. The higher conductivity found in compound **5′** compared that in **5** agrees with the shorter Na−Cl bond distances found in compound **5′** (Table 2).

The results observed in the electrical properties of compounds **1**−**5′** and also in **6**[7] clearly indicate that the chain structures observed in these compounds are very soft from the structural point of view and may be easily distorted. These tiny structural distortions produce important changes in the electrical conductivity because it strongly depends on the bridging bond lengths and angles, as observed in compounds **5** and **5′**. The softness of these structures is probably due to the poor coordinating capacity of chlorine and sulfur atoms with alkali-metal ions. The unusual presence of large hysteresis (up to ca. 60 K) in some of these compounds (mainly **1**, **5′**, and **6**) suggests that these distortions may have opposite propagation directions along the chain, leading to high activation energies for the distortions and, accordingly, to large thermal hysteresis.

Finally, it is interesting to compare the electrical conductivities of compounds **5** and **5′**, which present the same chain structure although with slightly diffferent Na−Cl and Na−S bond distances. As can be seen in Table 3, the electrical conductivity of compound **5′** is ca. 2 orders of magnitude higher than that of compound **5**. A close look at the bond distances displayed in Table 2 shows that the Na−S bond distances are quite similar (in **5**, these distances are 0.020 Å shorter), but the Na−Cl bond distances show the opposite trend with a much larger difference (in **5′**, these distances are 0.043 Å shorter). Furthermore, in **5′** there is one short Na−Cl distance of 3.085(10) Å, which is much shorter than those observed in **5** [3.177(4) and 3.203(4) Å; Table 2]. These shorter bond distances in **5′** must be at the origin of the higher electrical conductivity of **5′** compared to **5** because both chain structures are identical.

Magnetic Properties. Thermal variation of the molar magnetic susceptibility per $[Fe_2(SC_6H_2Cl_2S)_4]^{2-}$ dimer for compounds **1**−**5** shows very similar behaviors for all of the compounds (Figure 11). They all show very broad maxima at

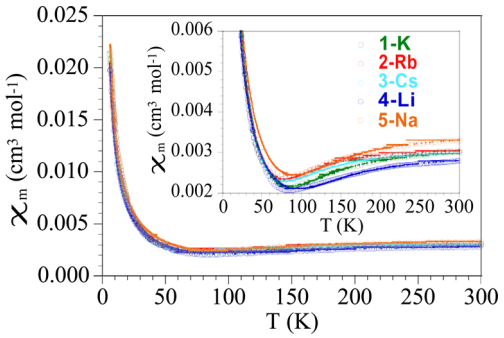

Figure 11. Thermal variation of the $\chi_m T$ product per $[Fe_2(SC_6H_2Cl_2S)_4]^{2-}$ dimer. The solid line is the best fit to the antiferromagnetic $S = {}^3/_2$ dimer model with a paramagnetic impurity. The inset shows the high-temperature data.

ca. 250−300 K, indicative of the presence of very strong intradimer antiferromagnetic Fe···Fe interactions. At lower temperatures, they all show minima at ca. 80 K and a divergence at lower temperatures corresponding to the contribution of a nonnegligible amount of paramagnetic impurities probably due to the presence of isolated $[Fe(SC_6H_2Cl_2S)_2]^-$ monomers and iron vacancies inside some dimers. Accordingly, in order to reproduce the magnetic properties of the five compounds, we have used a simple dimer model plus a paramagnetic contribution.[20] Because in these kinds of $[Fe_2(\text{dithiolato})_4]^{2-}$ dimers the ground spin state of the Fe^{III} ions may be ${}^1/_2$ or ${}^3/_2$, we have used both kinds of models to fit the magnetic data of compounds **1**−**5**. In all cases, the $S = {}^3/_2$ dimer model is the only one that reproduces satisfactorily the magnetic properties of compounds **1**−**5** with a reliable set of parameters (Table 4) and the following equation (the Hamiltonian is written as $-2JS_1S_2$):[20]

$$\chi = yC\frac{2e^{2x} + 10e^{6x} + 28e^{12x}}{1 + 3e^{2x} + 5e^{6x} + 7e^{12x}} + (1 - y)\frac{g^2}{8}S(S + 1),$$

$$\text{where } C = \frac{Ng^2\beta^2}{kT} \text{ and } \chi = \frac{J}{kT}$$

Thus, all the compounds show strong antiferromagnetic coupling constants in the range −229 to −303 cm^{-1}, *g* values

DOI: 10.1021/ic502789v
Inorg. Chem. 2015, 54, 2243−2252

Table 4. Magnetic Properties of Compounds 1−5

compound	S	g	J (cm^{-1})	c (%)[a]
1	$^3/_2$	2.004	−263	2.6
2	$^3/_2$	2.067	−229	2.9
3	$^3/_2$	2.053	−240	2.8
4	$^3/_2$	2.154	−303	2.4
5	$^3/_2$	2.133	−285	2.4

[a]Paramagnetic isolated Fe^{III} impurity.

close to 2, and paramagnetic Fe^{III} impurities of ca. 3% (solid lines in Figure 11). Note that these coupling constants are within the range found in other similar $[Fe_2(dithiolato)_4]^{2-}$ dimers characterized with similar $S = {}^3/_2$ dimer models.[21] The small amount of compound **5′** obtained in the reaction does not allow magnetic studies to be carried out on it.

CONCLUSIONS

Novel 1D alkali-iron dithiolene coordination polymers have been obtained by the direct reaction between $HSC_6H_2Cl_2SH$ and $FeCl_3{\cdot}6H_2O$ in the presence of aqueous solutions of the corresponding alkali-metal hydroxides (M = Li, Na, and K) or carbonates (M = Rb and Cs). These polymers are formed by $[Fe_2(SC_6H_2Cl_2S)_4]^{2-}$ entities connected by alkali-metal bimetallic units via M−Cl and M−S bonds. The only exception is the Li^+ derivative (**4**), where the $[Fe_2(SC_6H_2Cl_2S)_4]^{2-}$ entities are directly linked through Cl···Cl interactions. In the case of Na^+, we have been able to isolate two very closely related polymorphs (**5** and **5′**) that differ only in the orientation of the THF ligands coordinated to the Na^+ cations. However, this tiny difference leads to small changes in the Na···Cl and Na···S bond lengths that produce important changes in the electrical properties. All the compounds are semiconductors, although compounds **1** and **5′** present bistability at high temperatures with unusual large hysteresis of up to 60 K and exhibit intradimer strong antiferromagnetic Fe···Fe interactions.

ASSOCIATED CONTENT

Supporting Information

Crystallographic data in CIF format and additional figures of electrical characterization experiments. This material is available free of charge via the Internet at http://pubs.acs.org.

AUTHOR INFORMATION

Corresponding Author

*E-mail: esther.delgado@uam.es.

Notes

The authors declare no competing financial interest.

ACKNOWLEDGMENTS

Financial support from Spain's MICINN (Grants CTQ2011-26507 and MAT2013-46753-C2-1-P), Generalitat Valenciana (Projects PrometeoII/2014/076 and ISIC), and Factoria de Cristalización (CONSOLIDER-INGENIO 2010) is gratefully acknowledged.

REFERENCES

(1) (a) Robertson, N. Dithiolene Chemistry: Synthesis, Properties, and Applications. In *Coordination Chemistry Review*; Karlin, K. D., Stiefel, E. I., Cronin, L., Eds.; Elsevier BV: Amsterdam, The Netherlands, 2002; Vol. *227*, pp 93−127. (b) *Progress in Inorganic Chemistry*; John Wiley and Sons: New York, 2004; Vol. *52*. (c) Muller-Westerhoff, U. T.; Vance, B. In *Comprehensive Coordination Chemistry*, 1st ed.; Wilkinson, G., Gillard, R. D., McCleverty, J. A., Eds.; Pergamon Press: Oxford, U.K., 1987; Vol. 2. (d) Clemenson, P. I. *Coord. Chem. Rev.* **1990**, *106*, 171−203. (e) Belo, D.; Almeida, M. *Coord. Chem. Rev.* **2010**, *254*, 1479−1492. (f) Erzzaher, S.; Gogoll, A.; Bruhn, C.; Ott, S. *Chem. Commun.* **2010**, *46*, 5775−5577 and references cited therein. (g) Alcácer, L.; Novais, H. In *Extended Linear Chain Compounds*; Miller, J. S., Ed.; Plenum Press: New York, 1983; Chapter 6, pp 319−351. (h) Cassoux, P.; Valade, L.; Kobayashi, H.; Kobayashi, A.; Clark, R. A.; Underhill, A. E. *Coord. Chem. Rev.* **1991**, *110*, 115−160. (i) Sproules, S.; Wieghardt, K. *Coord. Chem. Rev.* **2010**, *254*, 1358−1382. (j) Garreau-de Bonneval, B.; Moineau-Chane Ching, K. I.; Alary, F.; Bui, T.-T.; Valade, L. *Coord. Chem. Rev.* **2010**, *254*, 1457−1467. (k) Alvarez, S.; Vicente, R.; Hoffmann, R. *J. Am. Chem. Soc.* **1985**, *107*, 6253. (l) Takaishi, S.; Hosoda, M.; Kajiwara, T.; Miyasaka, H.; Yamashita, M.; Nakanishi, Y.; Kitagawa, Y.; Yamaguchi, K.; Kobayashi, A.; Kitagawa, H. *Inorg. Chem.* **2009**, *48*, 9048−9050. (m) Ribas, X.; Dias, J. C.; Morgado, J.; Wusrt, K.; Santos, I. C.; Almeida, M.; Vidal-Gancedo, J.; Veciana, J.; Rovira, C. *Inorg. Chem.* **2004**, *43*, 3631−3641. (n) Llusar, R.; Uriel, S.; Vicent, C.; Clemente-Juan, J. M.; Coronado, E.; Gómez-García, C. J.; Braida, B.; Canadell, E. *J. Am. Chem. Soc.* **2004**, *126*, 12076−12083. (o) Llusar, R.; Triguero, S.; Polo, V.; Vicent, C.; Gómez-García, C. J.; Jeannin, O.; Fourmigue, M. *Inorg. Chem.* **2008**, *47*, 9400−9409. (p) Gushchin, A. L.; Llusar, R.; Vicent, C.; Abramov, P. A.; Gómez-García, C. J. *Eur. J. Inorg. Chem.* **2013**, *2013*, 2615−2622.

(2) (a) Ribas, X.; Dias, J.; Morgado, J.; Wurst, K.; Molins, E.; Ruiz, E.; Almeida, M.; Veciana, J.; Rovira, C. *Chem.—Eur. J.* **2004**, *10*, 1691−1704. (b) Baudron, S. A.; Hosseini, M. W. *Inorg. Chem.* **2006**, *45*, 5260−5262. (c) Roger, M.; Arliguie, T.; Thuéry, P.; Fourmigué, M.; Ephritikhine, M. *Inorg. Chem.* **2005**, *44*, 584−593. (d) Kong, L.-Q.; Dou, J.-M.; Li, D-Ch.; Wang, D.-Q. *J. Mol. Struct.* **2006**, *785*, 186−191. (e) Rabaca, S.; Almeida, M. *Coord. Chem. Rev.* **2010**, *254*, 1493−1508.

(3) Gao, X. K.; Dou, J.-M.; Li, D. C.; Dong, F. Y.; Wang, D. Q. *J. Mol. Struct.* **2005**, *733*, 181−186.

(4) Gao, X.-K.; Dou, J.-M.; Dong, F.-Y.; Li, D.-C.; Wang, D-Q. *J. Inorg. Organomet. Polym.* **2004**, *14*, 227−237.

(5) Sun, Y.-M.; Dong, F.-Y.; Dou, J.-M.; Li, D-Ch.; Gao, X.-K.; Wang, D.-Q. *J. Inorg. Organomet. Polym. Mater.* **2006**, *16*, 61−67.

(6) Bolligarla, R.; Das, S. K. *CrystEngComm* **2010**, *12*, 3409−3412.

(7) Amo-Ochoa, P.; Delgado, E.; Goméz-García, C. J.; Hernández, D.; Hernández, E.; Martin, A.; Zamora, F. *Inorg. Chem.* **2013**, *52*, 5943−5950.

(8) Farrugia, L. J. *J. Appl. Crystallogr.* **1999**, *32*, 837−838.

(9) *SHELXTL: Structure Determination Package*, version 6.10; Bruker Analytical X-ray Instruments: Madison, WI, 2000.

(10) *CRYSALISPRO*; Oxford Diffraction: Wroclaw, Poland, 2004.

(11) Sheldrick, G. M. *Acta Crystallogr.* **2008**, *A64*, 112−122.

(12) (a) Paluch, K. J.; Tajber, L.; McCabe, T.; O'Brien, J. E.; Corrigan, O. I.; Healy, A. M. *Eur. J. Pharm. Sci.* **2011**, *42*, 220−229. (b) Siewert, I.; Fitzpatrick, P.; Broomsgrove, A. E. J.; Kelly, M.; Vidovic, D.; Aldridge, S. *Dalton Trans.* **2011**, *40*, 10345−10350. (c) Sporer, C.; Ratera, I.; Ruiz-Molina, D.; Vidal Gancedo, J.; Wurst, K.; Jaitner, P.; Rovira, C.; Veciana, J. *J. Phys. Chem. Solids* **2004**, *65*, 753−758. (d) Becker, M.; Schulz, A.; Villinger, A.; Voss, K. *RSC Adv.* **2011**, *1*, 128−134. (e) Molcanov, K.; Kojic-Prodic, B.; Babic, D.; Zilic, D.; Rakvin, B. *CrystEngComm* **2011**, *13*, 5170−5178. (f) Kember, M. R.; Jutz, F.; Buchard, A.; White, A. J. P.; Williams, C. K. *Chem. Sci.* **2012**, *3*, 1245−1255. (g) Hu, J.; Barbour, L. J.; Gokel, G. W. *Chem. Commun.* **2002**, 1808−1809. (h) Sporer, C.; Ratera, I.; Ruiz-Molina, D.; Gancedo, J. V.; Ventosa, N.; Wurst, K.; Jaitner, P.; Rovira, C.; Veciana, J. *Solid State Sci.* **2009**, *11*, 786−792. (i) Osterloh, F.; Achim, C.; Holm, R. H. *Inorg. Chem.* **2001**, *40*, 224−232. (j) Smith, G. *Acta Crystallogr., Sect. E* **2014**, *70*, m23. (k) Gowda, B. T.; Babitha, K. S.; Svoboda, I.; Fuess, H. *Acta Crystallogr., Sect. E* **2007**, *63*, m2222. (l) Guinchard, X.; Bugaut, X.; Cook, C.; Roulland, E. *Chem.—Eur. J.* **2009**, *15*, 5793−5798.

DOI: 10.1021/ic502789v
Inorg. Chem. 2015, 54, 2243−2252

(13) Molcanov, K.; Kojic-Prodic, B.; Babic, D.; Zilic, D.; Rakvin, B. *CrystEngComm* **2011**, *13*, 5170−5178.
(14) (a) Smith, G.; Lynch, D. E. *Acta Crystallogr., Sect. C* **2014**, *70*, 606−612. (b) Smith, G. *Acta Crystallogr., Sect. E* **2013**, *69*, m628. (c) Levitskaia, T. G.; Bryan, J. C.; Sachleben, R. A.; Lamb, J. D.; Moyer, B. A. *J. Am. Chem. Soc.* **2000**, *122*, 554−562. (d) Smith, G. *Acta Crystallogr., Sect. E* **2013**, *69*, m22−m23. (e) Bröring, M.; Köhler, S.; Link, S.; Burghaus, O.; Pietzonka, C.; Kelm, H.; Krüger, H. *Chem.—Eur. J.* **2008**, *14*, 4006−4016. (f) Bryan, J. C.; Kavallieratos, K.; Sachleben, R. A. *Inorg. Chem.* **2000**, *39*, 1568−1572. (g) Cametti, M.; Nissinen, M.; Dalla Cort, A.; Rissanen, K.; Mandolini, L. *Inorg. Chem.* **2006**, *45*, 6099−6101.
(15) (a) Papadimitriou, C.; Veltsistas, P.; Marek, J.; Novosad, J.; Slawin, A. M. Z.; Woollins, J. D. *Inorg. Chem. Commun.* **1998**, *1*, 418−420. (b) Reiter, S. A.; Nogai, S. D.; Schmidbaur, H. *J. Coord. Chem.* **2005**, *58*, 81−87. (c) Brechin, E. K.; Gilby, L. M.; Gould, R. O.; Harris, S. G.; Parsons, S.; Winpenny, R. E. P. *J. Chem. Soc., Dalton Trans.* **1998**, 2657−2664. (d) Kunnas-Hiltunen, S.; Haukka, M.; Vepsalainen, J.; Ahlgren, M. *Dalton Trans.* **2010**, *39*, 5310−5318. (e) Chen, S.; Zhang, Z.; Zhou, Y.; Zhou, W.; Li, Y.; He, M.; Chen, Q.; Du, M. *Cryst. Growth Des.* **2011**, *11*, 4190−4197. (f) Molcanov, K.; Kojic-Prodic, B.; Meden, A. *Croat. Chem. Acta* **2009**, *82*, 387−396.
(16) Cerdeira, A. C.; Simao, D.; Santos, I. C.; Machado, A.; Pereira, L. C. J.; Waerenborgh, J. C.; Henriques, R. T.; Almeida, M. *Inorg. Chim. Acta* **2008**, *361*, 3836−3841.
(17) Alves, H.; Simao, D.; Novais, H.; Santos, I. C.; Gimenez-Saiz, C.; Gama, V.; Waerenborgh, J. C.; Henriques, R. T.; Almeida, M. *Polyhedron* **2003**, *22*, 2481−2488.
(18) Simao, D.; Ayllon, J. A.; Rabaca, S.; Figueira, M. J.; Santos, I. C.; Henriques, R. T.; Almeida, M. *Cryst. Eng. Commun.* **2006**, *8*, 658−661.
(19) (a) Chadwick, S.; Englich, U.; Ruhlandt-Senge, K. *Organometallics* **1997**, *16*, 5792−5803. (b) Reger, D. L.; Leitner, A.; Smith, M. D.; Tran, T. T.; Halasyamani, S. *Inorg. Chem.* **2013**, *52*, 10041−10051. (c) Weis, E. M.; Barnes, C. L.; Duval, P. B. *Inorg. Chem.* **2006**, *45*, 10126−10130. (d) Guzei, I. A.; Kim, M. H.; West, R. *J. Coord. Chem.* **2013**, *66*, 3722−3739. (e) Yu, X. Y.; Jin, G. X.; Weng, L. H. *Chem. Commun.* **2004**, 1542−1543. (f) Babo, J. M.; Wolff, K. K.; Schleid, T. *Z. Anorg. Allg. Chem.* **2013**, *639*, 2875−2881. (g) Emirdag-Eanes, M.; Ibers, J. A. *Inorg. Chem.* **2001**, *40*, 6910−6912. (h) Xu, W.; Vittal, J. J.; Puddephatt, R. J. *Inorg. Chem.* **1997**, *36*, 86−94. (i) Mi, J.-X.; Zhou, X.; Zhang, H.; Mao, S.-Y.; Zhao, J.-T. *Z. Kristallogr.—New Cryst. Struct.* **2004**, *219*, 93−94. (j) Morawitz, T.; Lerner, H.-W.; Bolte, M. *Acta Crystallogr.* **2007**, *E63*, m294−295. (k) Collin, J.; Daran, J.-C.; Schulz, E.; Trifonov, A. *Chem. Commun.* **2003**, 3048−3049. (l) Harder, S. *Organometallics* **2005**, *24*, 373−379.
(20) O'Connor, C. J. *Prog. Inorg. Chem.* **1982**, *29*, 203−283.
(21) (a) Rodrigues, J. V.; Santos, I. C.; Gama, V.; Henriques, R. T.; Waerenborgh, J. C.; Duarte, M. T.; Almeida, M. *J. Chem. Soc., Dalton Trans.* **1994**, 2655−2660. (b) Cerdeira, A. C.; Simao, D.; Santos, I. C.; Machado, A.; Pereira, L. C. J.; Waerenborgh, J. C.; Henriques, R. T.; Almeida, M. *Inorg. Chim. Acta* **2008**, *361*, 3836−3841. (c) Ray, K.; Bill, E.; Weyhermuller, T.; Wieghardt, K. *J. Am. Chem. Soc.* **2005**, *127*, 5641−5654. (d) Awaga, K.; Okuno, T.; Maruyama, Y.; Kobayashi, A.; Kobayashi, H.; Schenk, S.; Underhill, A. E. *Inorg. Chem.* **1994**, *33*, 5598−5600. (e) Deplano, P.; Leoni, L.; Mercuri, M. L.; Schlueter, J. A.; Geiser, U.; Wang, H. H.; Kini, A. M.; Manson, J. L.; Gomez-Garcia, C. J.; Coronado, E.; Koo, K. J.; Whangbo, M. H. *J. Mater. Chem.* **2002**, *12*, 3570−3577.

DOI: 10.1021/ic502789v
Inorg. Chem. 2015, 54, 2243−2252